Biodistribution and Radiation Dosimetry of ^{124}I-DPA-713, a PET Radiotracer for Macrophage-Associated Inflammation

Catherine A. Foss*[1,2], Donika Plyku*[1], Alvaro A. Ordonez[2,3], Julian Sanchez-Bautista[2,3], Hailey B. Rosenthal[1], Il Minn[1], Martin A. Lodge[1], Martin G. Pomper[1,2], George Sgouros[1], and Sanjay K. Jain[1–3]

[1]Russell H. Morgan Department of Radiology and Radiological Science, Johns Hopkins University School of Medicine, Baltimore, Maryland; [2]Center for Infection and Inflammation Imaging Research, Johns Hopkins University School of Medicine, Baltimore, Maryland; and [3]Department of Pediatrics, Johns Hopkins University School of Medicine, Baltimore, Maryland

Whole-body PET/CT was performed using ^{124}I-DPA-713, a radioligand for the 18-kDa translocator protein (TSPO), to determine biodistribution and radiation dosimetry. **Methods:** Healthy subjects aged 18–65 y underwent whole-body PET/CT either at 4, 24, and 48 h or at 24, 48, and 72 h after intravenous injection of ^{124}I-DPA-713. Time–activity curves were generated and used to calculate organ time-integrated activity coefficients for each subject. The resulting time-integrated activity coefficients provided input data for calculation of organ absorbed doses and effective dose for each subject using OLINDA. Subjects were genotyped for the *TSPO* polymorphism rs6971, and plasma protein binding of ^{124}I-DPA-713 was measured. **Results:** Three male and 3 female adults with a mean age of 40 ± 19 y were imaged. The mean administered activity and mass were 70.5 ± 5.1 MBq (range, 62.4–78.1 MBq) and 469 ± 34 ng (range, 416–520 ng), respectively. There were no adverse or clinically detectable pharmacologic effects in any of the 6 subjects. No changes in vital signs, laboratory values, or electrocardiograms were observed. ^{124}I-DPA-713 cleared rapidly (4 h after injection) from the lungs, with hepatic elimination and localization to the gastrointestinal tract. The mean effective dose over the 6 subjects was 0.459 ± 0.127 mSv/MBq, with the liver being the dose-limiting organ (0.924 ± 0.501 mGy/MBq). The percentage of free radiotracer in blood was approximately 30% at 30 and 60 min after injection. **Conclusion:** ^{124}I-DPA-713 clears rapidly from the lungs, with predominantly hepatic elimination, and is safe and well tolerated in healthy adults.

Key Words: pyrazolopyrimidine; macrophage; DPA-713; sarcoidosis; PET/CT

J Nucl Med 2018; 59:1751–1756
DOI: 10.2967/jnumed.117.207431

Macrophages are key components in chronic inflammatory diseases and belong to the mononuclear phagocyte system. Activated macrophages are critical in several diseases, such as tuberculosis and sarcoidosis (*1–3*), and a radiopharmaceutical imaging agent specific for macrophages would be clinically useful for the management and monitoring of diseases with macrophage-associated inflammation.

The translocator protein (TSPO) is an 18-kDa transmitochondrial membrane channel involved in cholesterol and other endogenous ligand transport (*4*). We have previously applied radioiodinated DPA-713 (*N,N*-diethyl-2-(4-methoxyphenyl)-5,7-dimethylpyrazolo[1,5-*a*] pyrimidine-3-acetamide), a low-molecular-weight pyrazolopyrimidine targeting TSPO, as an imaging agent for macrophage-associated inflammation. Although several TSPO-specific radioligands have been used to image inflammation (*5–8*), the short physical half-life of ^{11}C- and ^{18}F-labeled radioligands (20.3 and 109.7 min, respectively) enables visualization for only up to a few hours, which may be inadequate for washout of the radiotracer from TSPO-expressing healthy (e.g., pulmonary) tissues. Using experimental murine models of *Mycobacterium tuberculosis* infection within lung, we previously demonstrated that radioiodinated DPA-713 specifically accumulates in CD68-positive macrophages and phagocytic cells within tuberculous lesions after 24 h and can clearly delineate macrophage-associated pulmonary inflammation in live animals (*9,10*). Moreover, serial radioiodinated DPA-713 imaging correlated well with the bactericidal activity of tuberculosis treatments in mice (*10*). Here, we conducted the first, to our knowledge, studies on humans to assess the biodistribution and radiation dosimetry of ^{124}I-DPA-713 using PET/CT. These studies are important for future clinical translation of ^{124}I-DPA-713 as an imaging biomarker for macrophage-associated inflammation.

MATERIALS AND METHODS

This study was performed under a U.S. Food and Drug Administration exploratory investigational new drug application. The study protocol was approved by the Johns Hopkins University Institutional Review Board, and written informed was obtained from all subjects before enrollment.

Human Subjects

From June 2015 to May 2017, 6 healthy volunteers (3 male and 3 female) between 18 and 65 y old were recruited from the Johns Hopkins Hospitals (Table 1). The mean age of the subjects was 40 ± 19 y. Prestudy evaluation and poststudy follow-up (performed within 25 d of administration of the radiotracer) included a medical history of symptoms and a physical examination with vital signs, laboratory tests (a complete blood count with differential and a comprehensive metabolic panel to include blood urea nitrogen, creatinine, alkaline phosphatase, total bilirubin, and liver transaminase levels), and a screening electrocardiogram. However, given that all electrocardiograms were normal after imaging, the protocol was modified to remove poststudy

Received Jan. 9, 2018; revision accepted Mar. 16, 2018.
For correspondence or reprints contact: Sanjay K. Jain, 1550 Orleans St., CRB-II, Room 1.09, Baltimore, MD 21287.
E-mail: sjain5@jhmi.edu
*Contributed equally to this work.
Published online Apr. 26, 2018.

electrocardiography for the last 2 subjects. The eligibility criteria included a state of health as determined by a physician, as well as a laboratory evaluation within 28 d before enrollment showing normal liver function, a normal hemoglobin level (≥12.0 g/dL for men, ≥11.0 g/dL for women), a normal absolute neutrophil count (>1,000/mm^3), and a normal platelet count (>50,000/mm^3). Female subjects were screened for pregnancy and excluded if pregnant. Other exclusion criteria included the current use of antiinflammatory medications, regular nicotine or alcohol use, or active substance abuse. Subjects who had been treated with an investigational drug, investigational biologic, or investigational therapeutic device within 30 d before radiotracer administration were also excluded.

TSPO SNP (rs6971) Genotyping

Genotyping was performed as described previously (*11*). Briefly, whole blood from participants was collected and stored at 20°C. Genomic DNA was isolated from the whole blood using the PureGene Blood Core Kit C (Qiagen) according to the manufacturer's protocol for DNA purification from compromised samples. Genotypes were determined by performing polymerase chain reaction using the rs6971 TaqMan assay and the TaqMan Genotyping Master Mix (Applied Biosystems).

Radiotracer Administration

All subjects were given potassium iodide tablets (130 mg/d × 8 d) for thyroid blockade beginning 1 h before radiotracer injection. Vital signs were assessed before and 10 min after injection, and again after imaging, for any observable pharmacologic effects from radiotracer administration. ^{124}I-DPA-713 was manufactured under current good manufacturing practices by 3D Imaging, Ltd., according to the procedures described by Wang et al. (*12*). Radiochemical purity was greater than 90%, and specific activity was greater than 74 GBq/μmol. Solution volumes containing the target 74 MBq of activity ranged from 1.8 to 3.5 mL and were formulated in 20% ethanol in bicarbonate buffer, pH 8–9, and used as received. Bolus injection through an antecubital intravenous line was used for all subjects. A 10-mL sterile physiologic saline flush immediately followed tracer administration. A second contralateral antecubital line was used to withdraw 6–8 mL of whole blood 30 and 60 min after radiotracer injection for investigation of plasma protein binding.

PET/CT Protocol

A Siemens Biograph mCT scanner, equipped with high-performance lutetium oxyorthosilicate PET crystals and a CT component, was used to image all subjects from skull vertex to thighs in a supine position. A helical CT scan (120 kVp, 30 mAs reference, 0.5 s/rotation, 0.8 pitch) was acquired and used for attenuation correction of the PET data and anatomic coregistration to delineate organ boundaries. PET data were acquired at 7 overlapping bed positions at each of 4 time points: 4 h (n = 3), 24 h (n = 6), 48 h (n = 6), and 72 h (n = 3). Images were acquired in 3-dimensional mode at 5 min per bed position and were reconstructed as described previously (*13*), using 3-dimensional ordered-subset expectation maximization with time of flight and a correction for the prompt γ-emissions by ^{124}I. To obtain images in Bq/cm^3, the scanner was calibrated with a 20-cm-diameter, 20-cm-long ^{124}I-NaI water phantom using a Capintec CRC 15W dose calibrator with calibration 788 (*14*).

Time-Integrated Activity Coefficients (TIAC) and Absorbed Dose

Absorbed dose was calculated using the MIRD S value methodology (*15*) as implemented in the OLINDA/EXM software package (second-generation software package developed by Dr. Michael Stabin, Vanderbilt University) (*16*). The S value methodology provides the absorbed dose to a target tissue as the sum of dose contributions from all radioactivity-containing (source) tissues. The S value is usually obtained by a Monte Carlo simulation that is based on a standard or reference geometry for the subject and on the decay characteristics and emission spectrum of the radionuclide. S values for several source and target tissue combinations and a large number of radionuclides were previously incorporated into OLINDA/EXM (including ^{124}I). Once the absorbed dose for a series of organs is obtained, the effective dose can be calculated using tissue-weighting factors.

Volumes of interest (VOIs) were drawn manually, using the CT images as a reference, in Mirada XD3 (Mirada Medical) for dosimetry calculation. The VOIs were drawn on each respective CT image, providing 3 volumes for each organ corresponding to the 3 imaging time points. Attenuation-corrected PET data were coregistered with the CT images, and the drawn VOIs were applied to the PET data to generate the activity values in Bq/cm^3 per VOI. Time-integrated activity (TIA) curves were generated from the VOIs corresponding to each organ identified in the longitudinal PET imaging data as described above. In most cases, the VOI covered the entire organ volume. For cases in which the entire organ volume could not be separated from adjacent structures, a partial VOI was drawn to estimate the organ concentration. VOIs were drawn for whole-organ lung, spleen, kidney, gallbladder, liver, urinary bladder, pancreas, adrenal gland, small intestine, breast, thyroid, large intestine, thymus, stomach wall, uterus, and ovary and for the outer contour of the whole body. The gallbladder was not evident on the CT images of 2 subjects but was known to have been removed

TABLE 1
Subject Characteristics

Subject no.	Age (y)	TSPO genotype	Weight (kg)	Height (in*)	BMI	Injected activity (MBq)	Injected mass (ng)
F1	64	C/T	106.1	62	42.8	69.2	461
F2	43	C/T	97.5	63	38.1	71.6	476
F3	22	C/C	65.8	65	24.1	78.1	520
M1	59	C/T	78.0	73	22.7	71.6	477
M2	28	C/T	76.7	71.5	23.2	69.9	466
M3	22	C/C	71.7	72	21.4	62.4	416
Mean ± SD	40 ± 19		82.6 ± 15.7	68 ± 5	28.7 ± 9.2	70.5 ± 5.1	469 ± 34

*1 in = 2.54 cm.
BMI = body mass index; C/T = medium-affinity binder; C/C = high-affinity binder.

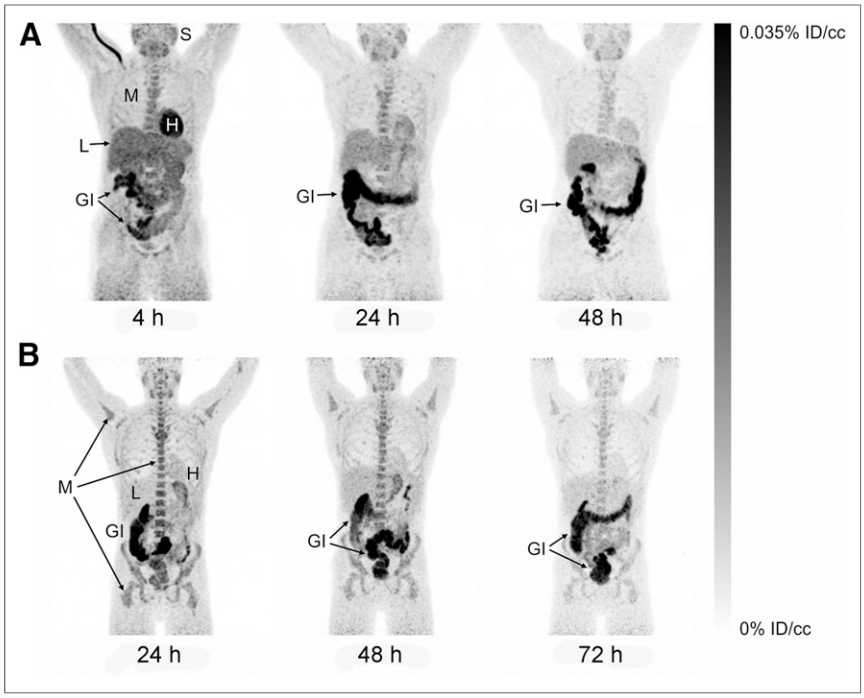

FIGURE 1. Maximum-intensity projections of biodistribution at 4–72 h after injection in 2 representative subjects. (A) At 4 h after injection, radiotracer uptake is primarily in heart, liver, salivary tissues, and bone marrow, and gastrointestinal clearance is readily observable. At 24 and 48 h, retention is reduced in all tissues except gastrointestinal tract. (B) At 24–72 h after injection, clearance is seen from most tissues but is slower from bone marrow and salivary tissues. However, signal in gastrointestinal tract is visible through 72 h. %ID/cc = percentage injected dose per cubic centimeter of tissue. GI = gastrointestinal tract; H = heart; L = liver; M = bone marrow; S = salivary tissues.

surgically in one of these two. A partial VOI was drawn for brain (the PET field of view was limited to the area from eyes to thighs), heart wall (the VOI was in only the left ventricular wall, to estimate the activity concentration in the heart wall), red marrow (subsampled in the L4–L5 vertebral bodies), muscle (left deltoid), and uterus (it could not always be visualized separately from surrounding organs). Supplemental Table 1 outlines the fractional masses of VOI and whole-organ reference masses for some tissues (supplemental materials are available at http://jnm.snmjournals.org). The thyroid for 1 subject (subject F3) was excluded from the analyses because she was found to have a history of thyroid dysfunction. A VOI of the thymus was drawn for subjects in whom a remnant could be identified. The activity concentration (Bq/cm^3) of the VOIs for each of the 3 measured time points was multiplied by the mean volume of the VOIs (average of the 3 VOIs drawn on each CT image) to calculate the total activity (Bq) according to Equation 1:

$$\text{Activity concentration}\left(\frac{\text{Bq}}{\text{cm}^3}\right) \times \text{mean VOI volume}\left(\text{cm}^3\right) = \text{total activity in VOI (Bq)}. \quad \text{Eq. 1}$$

The obtained time–activity curves were fit by using either a monoexponential function or a hybrid fit (trapezoidal + monoexponential function to the last 2 data points) and then integrated to obtain the TIA in the VOI. Whole-VOI TIAs were divided by subject-specific organ masses and multiplied by reference organ masses to obtain a scaled TIA for the VOI based on the standard adult male or female phantom as the subject case applied, according to Equation 2.

$$\text{Scaled TIA (Bq-h)} = \frac{\text{TIA}_{\text{drawn}_{\text{VOI(Bq-h)}}}}{M_{\text{drawn}_{\text{VOI}}}(\text{g})} \times M_{\text{ref(g)}}, \quad \text{Eq. 2}$$

where the mass of the drawn VOI was calculated as the product of the mean volume of the 3 drawn VOIs on each CT image by the reference-tissue densities from International Commission on Radiological Protection publication 23 (*17*) or 89 (*18*), and the reference organ mass (M_{ref}) was derived from publication 60 (*19*) as implemented in OLINDA/EXM. The resulting scaled organ TIAs were divided by the injected activity to obtain the TIAC for each source organ. The TIAC of the remainder of the body was calculated by subtracting the sum of the TIACs for all organ of interest from the TIAC for the whole available field of view (from skull vertex to thighs). The obtained TIACs were used as input to OLINDA/EXM to obtain the absorbed dose to most target organs. The MIRD bladder model (*20*) was used to calculate the absorbed dose to the bladder with a voiding interval of 4 h, the biologic clearance half-life, and a fraction of 1. The adult female or male phantom was interchangeably used according to the sex of the subject, and absorbed dose was calculated for ^{124}I using the calculated TIACs for the source organs that each phantom requires as input.

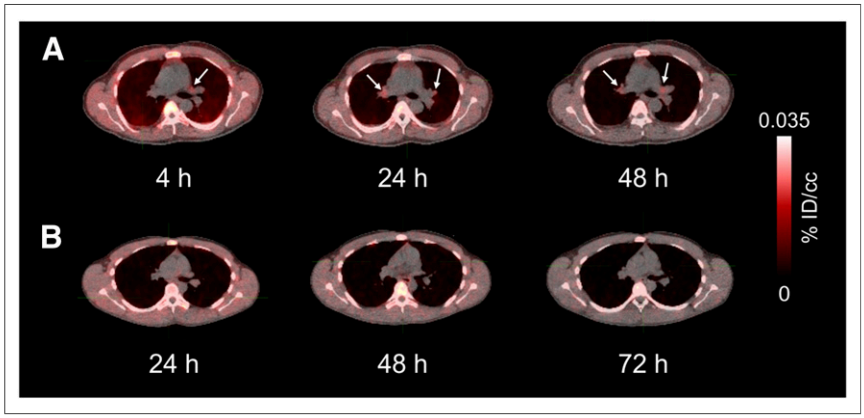

FIGURE 2. Biodistribution in lungs and mediastinum 4–72 h after injection as seen on transaxial PET/CT images from subjects A and B of Figure 1. Mediastinal uptake is low in A (arrows) but absent from B. %ID/cc = percentage injected dose per cubic centimeter of tissue.

Plasma Protein Binding

Plasma protein binding was determined by isolation of fresh subject plasma by centrifugation (1,500*g* for 10 min at 4°C) followed by loading of a 0.5-mL aliquot of plasma into an Amicon Ultra-0.5 30-kDa purification device,

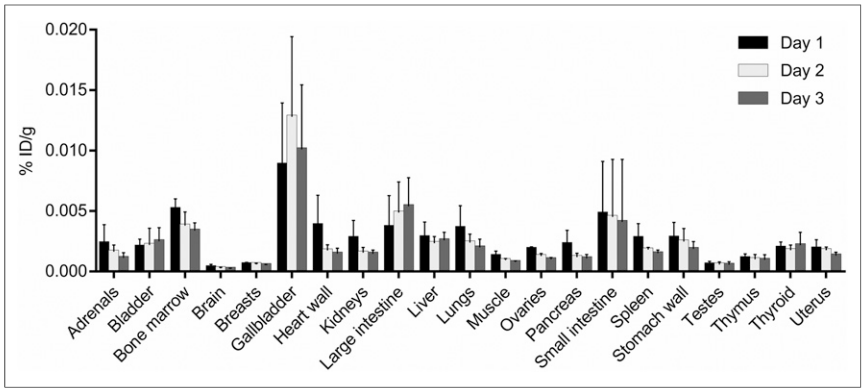

FIGURE 3. Mean and SD for physical decay–corrected biodistribution (biodistribution assuming no physical decay of radionuclide) on days 1, 2, and 3. %ID/g = percentage injected dose per cubic centimeter of tissue.

which was centrifuged at 14,000*g* for 30 min at room temperature. The filtrate was then saved, and the remaining supernatant was recovered by centrifugation at 1,000*g* for 2 min. The filtrate, recovered supernatant, and filter itself were counted separately in a Wallac Compugamma automated γ-counter. The filtrate represented free, or unbound, radiotracer whereas the supernatant represented protein-bound radiotracer (≥30 kDa protein-bound). The filter device represented nonspecific binding, and this value was subtracted from both supernatant and filtrate values. Values were expressed as free radiotracer.

RESULTS

The mean administered activity and mass were 70.5 ± 5.1 MBq (range, 62.4–78.1 MBq) and 469 ± 34 ng (range, 416–520 ng), respectively. There were no adverse or clinically detectable pharmacologic effects in any of the subjects. No significant changes in vital signs, laboratory values, or electrocardiograms were observed.

Representative maximum-intensity projections of radiotracer biodistribution are shown in Figure 1. ^{124}I-DPA-713 cleared rapidly from the lungs, with substantial hepatic elimination and localization to the gastrointestinal tract. The images in Figure 1, of 2 subjects earlier and later after injection, illustrate cardiac and liver uptake at 4 h and heart, lung, liver, and kidney washout at later times in both subjects. Marrow, salivary gland, and gastrointestinal clearance dominated from 24 h onward. Salivary gland uptake might represent transient uptake of metabolically liberated radioiodide. Figure 2 demonstrates clear lung fields in these same 2 subjects even at 4 h. Physical decay–corrected biodistribution for various organs is shown in Figure 3.

TIAC and Absorbed Dose

The calculated TIACs are shown in Table 2. For both sexes, the longest TIACs were in muscle (11.8 ± 3.83 h and 18.6 ± 3.44 h in women and men, respectively), liver (6.96 ± 4.39 h and 4.57 ± 1.25 h, respectively), marrow (4.45 ± 0.54 h and 1.27 ± 0.70 h, respectively), and lungs (2.02 ± 1.22 h and 2.95 ± 0.87 h, respectively). The tissues with the most similar and the most different TIACs between female and male subjects were stomach wall (~78% difference) and thymus (0.3% difference). Figure 4 and Table 3 show the absorbed dose in mGy/MBq. Liver, followed by uterus and lower-large-intestine wall, received the highest absorbed dose and was the dose-limiting organ, with a mean absorbed dose of 0.924 mGy/MBq (3.42 rem/mCi). Data for individual subjects are shown in Supplemental Tables 2 and 3. Qualitatively, absorbed doses and TIACs did not seem dependent on the rs6971 genotype of the subject.

Plasma Protein Binding Assays

The mean percentages of free radiotracer in male and female subjects were 29% and 32%, respectively, at both 30 and 60 min. Subject M2 unexpectedly displayed very low free radiotracer at 30 and 60 min, at 0.9% and 1.6%, respectively, and these values were excluded from the means (Supplemental Table 4).

DISCUSSION

Several radioligands, including those targeting inducible nitric oxide synthase (*21*), folate receptor-β (*22,23*), CD206 (*24,25*), and LOX-1 (*26–28*), have been developed to visualize macrophages, and several of these have also been used to image acute inflammation. Though present ubiquitously, TSPO expression is elevated in immunologically activated leukocytes such as microglia and macrophages (*29*) and has been used as a molecular target for imaging of neuroinflammation (*30–33*).

TABLE 2
TIACs

Site	TIAC (h)
Brain	0.275 ± 0.136
Lungs	1.647 ± 0.981
Spleen	0.267 ± 0.170
Kidneys	0.386 ± 0.120
Gallbladder	0.073 ± 0.042
Liver	5.766 ± 3.170
Heart wall	0.423 ± 0.175
Bladder	0.738 ± 0.219
Pancreas	0.096 ± 0.041
Red marrow	3.698 ± 1.048
Adrenal glands	0.014 ± 0.008
Small intestine	1.363 ± 0.499
Breasts	0.195 ± 0.054
Testes	0.029 ± 0.015
Thyroid	0.048 ± 0.025
Large intestine	1.727 ± 0.849
Thymus	0.018 ± 0.008
Muscle	15.191 ± 4.921
Stomach wall	0.309 ± 0.212
Uterus	0.083 ± 0.019
Ovaries	0.015 ± 0.010
Whole body	59.844 ± 18.115
Remainder of body	27.676 ± 18.748

Data are mean ± SD.

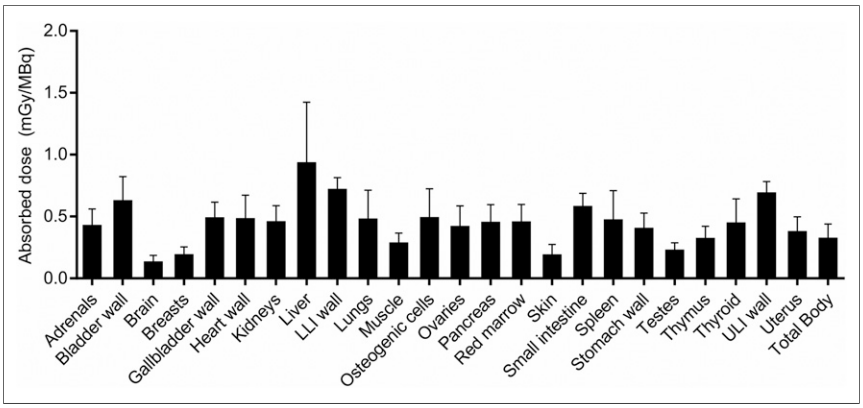

FIGURE 4. Mean and SD for organ-absorbed doses. LLI = lower large intestine; ULI = upper large intestine.

Recently, several TSPO-specific radioligands have also been used to detect chronic inflammation in peripheral tissues (*5–8*). However, the short physical half-life of ^{18}F- and ^{11}C-labeled TSPO-specific radioligands enables visualization of processes for only up to a few hours, which may be inadequate for washout of the radiotracer from TSPO-expressing healthy tissues. The distribution of ^{124}I-DPA-713 at 4, 24, 48, and 72 h after injection was different from that of other reported TSPO-targeted radioligands as typically described shortly after administration (*34*) and was instead consistent with the distribution of active and resting monocyte-lineage cells. Notably, at and beyond 24 h after injection in healthy subjects, the dominant uptake was observed in red marrow, putatively by macrophage-replenishing mononuclear phagocyte progenitors (*35*) along with residual TSPO-rich heart and liver uptake. Salivary gland uptake likely represented transient uptake of metabolized radioiodide, though metabolites were not assayed. Gastrointestinal uptake appeared to represent hepatobiliary radiotracer clearance.

TABLE 3
Absorbed Dose Estimates

Site	Estimate (mGy/MBq)
Adrenals	0.418 ± 0.143
Brain	0.122 ± 0.064
Breasts	0.181 ± 0.074
Gallbladder wall	0.480 ± 0.136
Lower large intestinal wall	0.709 ± 0.105
Small intestine	0.571 ± 0.117
Stomach wall	0.394 ± 0.134
Upper large intestinal wall	0.681 ± 0.102
Heart wall	0.472 ± 0.201
Kidneys	0.448 ± 0.139
Liver	0.924 ± 0.501
Lungs	0.470 ± 0.243
Muscle	0.276 ± 0.090
Ovaries	0.409 ± 0.177
Pancreas	0.442 ± 0.154
Red marrow	0.446 ± 0.151
Osteogenic cells	0.481 ± 0.243
Skin	0.179 ± 0.095
Spleen	0.463 ± 0.246
Testes	0.218 ± 0.069
Thymus	0.312 ± 0.108
Thyroid	0.438 ± 0.204
Urinary bladder wall	0.618 ± 0.204
Uterus	0.367 ± 0.131
Total body	0.315 ± 0.125
Effective dose (mSv/MBq)	0.459 ± 0.127

Data are mean ± SD.

The tissues displaying the longest retention included liver, lung, marrow, and muscle. Isotope half-life (4.2 d) and lipophilic pharmacokinetics (calculated logD, 3.75) contribute to these relatively large TIACs. Lengthy retention in each tissue, excluding muscle, is expected because of specific uptake in resident macrophages or progenitor cells, that is, Kupffer cells in liver, alveolar macrophages and type II pneumocytes in lung, and mononuclear phagocyte progenitors in marrow, as well as hepatic and gastrointestinal elimination. Persistence in muscle may be due to the lipophilic nature of this radiotracer and to the fact that approximately 65%–70% of the radiotracer is bound by plasma proteins, leading to slower clearance from muscle (*36*). Calculated radiation doses were higher for ^{124}I-DPA-713 than for ^{18}F-FDG but were similar to other radiotracers labeled with ^{124}I, such as ^{124}I-MIP-109, a highly hydrophilic radiotracer targeting prostate-specific membrane antigen (*37*). In these cases, it is the radionuclide half-life that largely contributes to these relatively high absorbed doses. Variability in absorbed doses was observed among subjects within and between the sexes, and the liver was the dose-limiting organ. Subject M2 also exhibited very high plasma protein binding, though the organ-specific TIACs were comparable to those of the other subjects. Given the long uptake times and sequestration of radiotracer inside selective cells, we believe that protein binding may have less of an effect on uptake than in acute equilibrium binding studies. Finally, whereas absorbed doses and TIACs (qualitatively) were not dependent on the rs6971 genotype, no subject was found to have the T/T variant. This is a limitation of the current study because Coughlin et al. previously demonstrated that subjects with the T/T variant had substantially lower ^{11}C-DPA-713 binding than subjects with other variants (*11*). Future ^{124}I-DPA-713 PET studies that include subjects with the T/T variant could provide clarity on this issue.

At 4 h after injection, the lungs displayed minimal uptake whereas the heart displayed the highest nonclearance uptake. For the purpose of imaging macrophages localized in the lungs, and cervical and thoracic lymph nodes, a 24-h uptake period is most likely sufficient for high-contrast viewing. Fluorescence-assisted cell sorting was previously used to assay cell-specific uptake and demonstrated that a fluorescent analog of DPA-713 (DPA-713-IRDye680LT (*9,38*) and, by analogy, radioiodinated

DPA-713) is retained primarily by macrophage and dendritic cell populations (*10*).

CONCLUSION

^{124}I-DPA-713 clears rapidly from the lungs, with predominantly hepatic elimination, and is safe and well tolerated in healthy adults. These studies are important for future clinical translation of ^{124}I-DPA-713 as an imaging biomarker for macrophage-associated inflammation.

DISCLOSURE

This study was funded by the National Institutes of Health (grant R01-HL131829 to Sanjay Jain, AIDS Clinical Trials Group award UM1-AI068636 from Brigham and Women's Hospital as a supplement to Sanjay Jain, and salary support from grant P41-EB024495 to Martin Pomper). No other potential conflict of interest relevant to this article was reported.

ACKNOWLEDGMENTS

We thank each of our human subjects for volunteering for the study, and we thank the Johns Hopkins PET Center staff for performing the imaging.

REFERENCES

1. Qualls JE, Murray PJ. Immunometabolism within the tuberculosis granuloma: amino acids, hypoxia, and cellular respiration. *Semin Immunopathol.* 2016;38:139–152.
2. Kataria YP, Holter JF. Immunology of sarcoidosis. *Clin Chest Med.* 1997;18: 719–739.
3. Jewell DP, Patel C. Immunology of inflammatory bowel disease. *Scand J Gastroenterol Suppl.* 1985;114:119–126.
4. Rupprecht R, Papadopoulos V, Rammes G, et al. Translocator protein (18 kDa) (TSPO) as a therapeutic target for neurological and psychiatric disorders. *Nat Rev Drug Discov.* 2010;9:971–988.
5. Bird JL, Izquierdo-Garcia D, Davies JR, et al. Evaluation of translocator protein quantification as a tool for characterising macrophage burden in human carotid atherosclerosis. *Atherosclerosis.* 2010;210:388–391.
6. Zheng J, Boisgard R, Siquier-Pernet K, Decaudin D, Dolle F, Tavitian B. Differential expression of the 18 kDa translocator protein (TSPO) by neoplastic and inflammatory cells in mouse tumors of breast cancer. *Mol Pharm.* 2011;8:823–832.
7. Kam WW-Y, Meikle SR, Zhou H, et al. The 18 kDa translocator protein (peripheral benzodiazepine receptor) expression in the bone of normal, osteoprotegerin or low calcium diet treated mice. *PLoS One.* 2012;7:e30623.
8. Hatori A, Yui J, Yamasaki T, et al. PET imaging of lung inflammation with [^{18}F] FEDAC, a radioligand for translocator protein (18 kDa). *PLoS One.* 2012;7:e45065.
9. Foss CA, Harper JS, Wang H, Pomper MG, Jain SK. Noninvasive molecular imaging of tuberculosis-associated inflammation with radioiodinated DPA-713. *J Infect Dis.* 2013;208:2067–2074.
10. Ordonez AA, Pokkali S, DeMarco VP, et al. Radioiodinated DPA-713 imaging correlates with bactericidal activity of tuberculosis treatments in mice. *Antimicrob Agents Chemother.* 2015;59:642–649.
11. Coughlin JM, Wang Y, Ma S, et al. Regional brain distribution of translocator protein using [^{11}C]DPA-713 PET in individuals infected with HIV. *J Neurovirol.* 2014;20:219–232.
12. Wang H, Pullambhatla M, Guilarte TR, Mease RC, Pomper MG. Synthesis of [^{125}I]iodoDPA-713: a new probe for imaging inflammation. *Biochem Biophys Res Commun.* 2009;389:80–83.
13. Hudson HM, Larkin RS. Accelerated image reconstruction using ordered subsets of projection data. *IEEE Trans Med Imaging.* 1994;13:601–609.
14. Beattie BJ, Pentlow KS, O'Donoghue J, Humm JL. A recommendation for revised dose calibrator measurement procedures for ^{89}Zr and ^{124}I. *PLoS One.* 2014; 9:e106868.
15. Bolch WE, Eckerman KF, Sgouros G, Thomas SR. MIRD pamphlet no. 21: a generalized schema for radiopharmaceutical dosimetry—standardization of nomenclature. *J Nucl Med.* 2009;50:477–484.
16. Stabin MG, Sparks RB, Crowe E. OLINDA/EXM: the second-generation personal computer software for internal dose assessment in nuclear medicine. *J Nucl Med.* 2005;46:1023–1027.
17. Snyder WS, Cook MJ, Nasset ES, Karhausen LR, Howells GP, Tipton IH. *ICRP Publication 23, Report of the Task Group on Reference Man.* Elmsford, NY: International Commission on Radiological Protection; 1975:97–200.
18. Basic anatomical and physiological data for use in radiological protection: reference values—a report of age- and gender-related differences in the anatomical and physiological characteristics of reference individuals. ICRP publication 89. *Ann ICRP.* 2002;32:5–265.
19. 1990 Recommendations of the international commission on radiological protection. *Ann ICRP.* 1991;21:1–201.
20. Thomas SR, Stabin MG, Chen CT, Samaratunga RC. MIRD pamphlet no. 14 revised: a dynamic urinary bladder model for radiation dose calculations. Task Group of the MIRD Committee, Society of Nuclear Medicine. *J Nucl Med.* 1999;40(suppl):102S–123S.
21. Huang HJ, Isakow W, Byers DE, et al. Imaging pulmonary inducible nitric oxide synthase expression with PET. *J Nucl Med.* 2015;56:76–81.
22. Chandrupatla DM, Jansen G, Vos R, et al. In-vivo monitoring of anti-folate therapy in arthritic rats using [^{18}F]fluoro-PEG-folate and positron emission tomography. *Arthritis Res Ther.* 2017;19:114.
23. Han W, Zaynagetdinov R, Yull FE, et al. Molecular imaging of folate receptor beta-positive macrophages during acute lung inflammation. *Am J Respir Cell Mol Biol.* 2015;53:50–59.
24. Zanni MV, Toribio M, Wilks MQ, et al. Application of a novel CD206+ macrophage-specific arterial imaging strategy in HIV-infected individuals. *J Infect Dis.* 2017;215:1264–1269.
25. Kim EJ, Kim S, Seo HS, et al. Novel PET imaging of atherosclerosis with ^{68}Ga-labeled NOTA-neomannosylated human serum albumin. *J Nucl Med.* 2016;57:1792–1797.
26. Luo B, Wen S, Chen YC, et al. LOX-1-targeted iron oxide nanoparticles detect early diabetic nephropathy in db/db mice. *Mol Imaging Biol.* 2015;17:652–660.
27. Wen S, Liu DF, Cui Y, et al. In vivo MRI detection of carotid atherosclerotic lesions and kidney inflammation in ApoE-deficient mice by using LOX-1 targeted iron nanoparticles. *Nanomedicine.* 2014;10:639–649.
28. Li D, Patel AR, Klibanov AL, et al. Molecular imaging of atherosclerotic plaques targeted to oxidized LDL receptor LOX-1 by SPECT/CT and magnetic resonance. *Circ Cardiovasc Imaging.* 2010;3:464–472.
29. Zavala F, Haumont J, Lenfant M. Interaction of benzodiazepines with mouse macrophages. *Eur J Pharmacol.* 1984;106:561–566.
30. Cagnin A, Gerhard A, Banati RB. The concept of in vivo imaging of neuroinflammation with [^{11}C](R)-PK11195 PET. *Ernst Schering Res Found Workshop.* 2002:179–191.
31. Endres CJ, Pomper MG, James M, et al. Initial evaluation of ^{11}C-DPA-713, a novel TSPO PET ligand, in humans. *J Nucl Med.* 2009;50:1276–1282.
32. Fujimura Y, Zoghbi SS, Simeon FG, et al. Quantification of translocator protein (18 kDa) in the human brain with PET and a novel radioligand, ^{18}F-PBR06. *J Nucl Med.* 2009;50:1047–1053.
33. Gerhard A, Pavese N, Hotton G, et al. In vivo imaging of microglial activation with [^{11}C](R)-PK11195 PET in idiopathic Parkinson's disease. *Neurobiol Dis.* 2006;21:404–412.
34. Turkheimer FE, Rizzo G, Bloomfield PS, et al. The methodology of TSPO imaging with positron emission tomography. *Biochem Soc Trans.* 2015;43:586–592.
35. Bain CC, Bravo-Blas A, Scott CL, et al. Constant replenishment from circulating monocytes maintains the macrophage pool in the intestine of adult mice. *Nat Immunol.* 2014;15:929–937.
36. Kakutani T, Sumimoto E, Hashida M. Effect of plasma protein binding on drug disposition in muscle tissue: application of statistical moment analysis and network theory to in situ local single-pass perfusion system. *J Pharmacokinet Biopharm.* 1988;16:129–149.
37. Zechmann CM, Afshar-Oromieh A, Armor T, et al. Radiation dosimetry and first therapy results with a ^{124}I/^{131}I-labeled small molecule (MIP-1095) targeting PSMA for prostate cancer therapy. *Eur J Nucl Med Mol Imaging.* 2014;41: 1280–1292.
38. Foss CA, Bedja D, Mease RC, et al. Molecular imaging of inflammation in the ApoE −/− mouse model of atherosclerosis with IodoDPA. *Biochem Biophys Res Commun.* 2015;461:70–75.